PAPER

Ultrathin insulating under-layer with a hematite thin film for enhanced photoelectrochemical (PEC) water splitting activity†

Myung Jong Kang and Young Soo Kang*

An ultrathin SiO_2 under-layer was inserted between the FTO substrate and the Ti-doped hematite film to suppress the reverse electron recombination from the FTO substrate to the hematite layer for improved photoelectrochemical activity of the hematite film during the photoelectrochemical (PEC) water splitting reaction. The reverse current of the SiO_2 under-layered hematite thin film decreased from -0.075 mA cm^{-2} to -0.035 mA cm^{-2}, with enhanced interfacial charge transfer and internal charge transport efficiencies. The hematite film with the ultrathin SiO_2 under-layer showed a promising photocurrent density of 0.76 mA cm^{-2} at 1.23 V *vs.* RHE under 1 sun illumination without hole scavenger materials during the PEC water splitting reaction.

Introduction

Solar water splitting, producing hydrogen gas from water using solar energy, is receiving attention as an environmentally friendly renewable energy.[1] Photoelectrochemical (PEC) water splitting, generating oxygen and hydrogen by splitting water, is the half reaction of artificial photosynthesis.[2,3] The materials for PEC water splitting require small band gaps for a good light absorption efficiency,[4] long diffusion lengths for electron–hole mobility and appropriate band positions for water splitting.[5] However, no material has been reported that fulfils all these requirements for effective PEC water splitting. Recently, plenty of semiconductor metal oxide materials, such as ZnO, TiO_2, $BiVO_4$ and Fe_2O_3, have been considered as candidate materials.[5–7] Hematite (α-Fe_2O_3) is one of the promising PEC water splitting materials due to the fact that it is an abundant and low cost material with a suitable band gap ($\sim$2.1 eV)[8] for water oxidation in the visible light range and a good chemical stability. Theoretically, an ideal hematite photoanode can attain a PEC performance of 12 mA cm^{-2}.[9] However, the latest study still could not reach the theoretical maximum PEC performance due to poor optical absorption, short diffusion lengths (2–4 nm),[10] short life times of the excited electrons (less than 10 ps)[11] and poor oxygen evolution kinetics. These disadvantages result in a poor PEC activity of hematite during the PEC water splitting reaction.

To improve the photoelectrochemical activity of hematite, previous approaches have involved doping other metals into hematite to control the band gap energy, constructing p–n junctions to suppress the charge recombination of hematite[12] and attaching co-catalysts to the surface of the hematite film to increase the charge separation ability.[13] Doping higher or lower valence band metal ions into hematite can adjust the conduction band position, valence band position and band gap energy of hematite. Moreover, through attaching oxygen evolution catalysts (OECs), like IrO_x,[14] cobalt phosphate (Co-Pi)[15,16] and Pt,[17] hematite can have suitable characteristics for efficient solar water splitting and an enhanced conductivity for a better PEC activity.

There are plenty of methods for preparing hematite thin films for solar water splitting, including hydrothermal methods,[18,19] ALD methods,[20] plasma enhanced chemical vapour deposition (PECVD)[21] and atmospheric pressure chemical vapor deposition (APCVD).[22] Furthermore, Yat Li *et al.* reported that the preparation of hematite thin films with Ti doping by the facile deposition and annealing (DA) method resulted in an enhanced PEC activity.[23] After the report on Ti doping into hematite, there were several reports on other transition elements, such as Zn, Pt and Si, being doped into hematite films, which resulted in enhanced PEC activities of hematite.[22,24,25]

Another approach to increase the PEC activity of hematite thin films is focused on modifying the interface junction between the FTO substrate and the hematite thin film layer. Mathews *et al.* introduced niobium oxide (Nb_2O_5) as an under-layer to the hematite film and achieved a maximum photocurrent density of *ca.* 0.1 mA cm^{-2} at 1.23 V *vs.* RHE without hole

Korea Center for Artificial Photosynthesis, Sogang University, Department of Chemistry, Seoul, 121-742, Korea. E-mail: yskang@sogang.ac.kr

This journal is © The Royal Society of Chemistry 2015

J. Mater. Chem. A, 2015, **3**, 15723–15728 | **15723**

scavenger materials.[26] Recently, Zhang *et al.* introduced a thin TiO_2 under-layer between the hematite film and the Pt-coated fluorine doped tin oxide (FTO) substrate, leading to an enhanced charge transport in the hematite thin film. They recorded a photocurrent density of 0.4 mA cm^{-2} at 1.23 V *vs.* RHE at the PEC water splitting potential.[27]

Herein, we report a facile and effective method to enhance the PEC water splitting activity of a hematite film by introducing an ultrathin SiO_2 under-layer between the FTO substrate and hematite film using the DA method. An oxygen plasma treatment process was carried out to make the FTO surface more hydrophilic and to achieve better interactions between the precursor solution and the FTO substrate during the hematite thin film preparation. A spin-coating method was used for the deposition of the Fe precursor solution to achieve a higher uniformity of the thin film. Ti was also doped into hematite to enhance the PEC activity of the hematite thin film. Finally, by introducing an ultrathin SiO_2 under-layer between the FTO substrate and hematite film, the reverse electron recombination pathway from the FTO substrate to the Ti-doped hematite thin film was suppressed without any decrease in the forward electron flow, leading to enhanced charge transport and interfacial charge transfer efficiencies, which resulted in an increase in the PEC activity of the hematite thin film without any hole scavenger materials and co-catalysts in the PEC water splitting reaction.

Experimental

Materials and synthesis

Synthesis of pure α-Fe$_2$O$_3$ and the Ti doped α-Fe$_2$O$_3$ film. An ethanol solution containing 20 mM FeCl$_3$ (97%, Sigma-Aldrich) was dropped and spin coated at 1200 rpm speed on the surface of the oxygen plasma treated FTO substrate. The spin coated sample on the FTO substrate was heated at 300 °C on the surface of a hot-plate for 5 min. These two steps were comprised of a sequence of deposition and annealing (DA) cycles. After 10 DA cycles, the sample was annealed at 550 °C in a furnace for 3 h to make the α-Fe$_2$O$_3$ thin film. For the preparation of α-Fe$_2$O$_3$:Ti, an ethanol solution containing 20 mM FeCl$_3$ was prepared and titanium butoxide (97%, Sigma-Aldrich) as the Ti precursor was added to the prepared solution so that the atomic ratio of Ti to Fe was 10%. To prevent reactions that cause metallic Ti to change to titanium dioxide, 0.35 ml of saturated HCl (37.2 wt%, Daejung Chemical) was added per 100 ml of solution. The solution was stirred continuously overnight and spin coated at 1200 rpm speed on the surface of the oxygen plasma treated FTO substrate. This was then heated at 300 °C on the surface of a hot plate for 5 min. After 10 DA cycles, the sample was annealed at 550 °C in the furnace for 3 h.

Synthesis of the SiO$_2$ under-layered Ti doped α-Fe$_2$O$_3$ film

A butanol solution containing 0.45 M tetraethyl orthosilicate (98%, Sigma-Aldrich) was spin coated at 1200 rpm on the surface of the oxygen plasma treated FTO substrate. This was then heated at 300 °C on the hot plate surface for 5 min and annealed at 500 °C in the furnace for 3 h to make the silica layer. A mixed solution of 20 mM FeCl$_3$ and titanium butoxide was prepared in ethanol, with an atomic ratio of Ti to Fe of 10%. 0.35 ml of saturated HCl was added per 100 ml of solution to prevent oxidation of the Ti precursor. The solution was spin coated on the surface of the SiO$_2$ under-layered FTO substrate at 1200 rpm and heated at 300 °C for 5 min. The sample was annealed again at 550 °C for 3 h in the furnace after 10 DA cycles.

Characterization of the structure and optical properties

The layered structure analysis was performed with Cs-corrected transmission electron microscopy (Cs corrected-TEM: JEOL, JEM-ARM200F), including an EDXS analysis system (Bruker Quantax 400) with an incident electron beam at 200 kV. To clarify the binding state of each atom, X-ray photoelectron spectroscopy (XPS) spectra were obtained with an Al Kα source (Sigma probe, ThermoVG, United Kingdom), including depth profiling. The local binding state of each atom was investigated by X-ray Absorption Fine Structure (XAFS) analysis using a synchrotron radiation beam in the Pohang Accelerator Laboratory (PAL) 1D beam line, and analysed by computational calculations with the IFEFFIT algorithm. The optical absorbance of each sample was also measured by UV-Vis spectroscopy (Agilent Carry 5000) with a universal measurement accessory. Surface images and the average surface roughness values of the hematite thin films were obtained by atomic force microscopy (Pucotech, PUCOstation STD).

The photocurrent density, electrochemical impedance spectroscopy (EIS), incident photon to current conversion efficiency (IPCE) and transient *J–V* curves were measured at room temperature, using a photoelectrochemical (PEC) measurement system (Ivium, Compactstat) with a three electrode electrochemical system, 1.0 M NaOH electrolyte (pH 13.6), and front side illumination, which simulated sunlight from a 300 W xenon lamp (Asahi Spectra HAL-320, ozone free, spectrum is shown in Fig. S1†), with AM 1.5G conditions and an intensity of light of 1 sun (100 mW cm^{-2}, spectrally corrected). Platinum wire was used as the counter electrode. The potential was measured with a Ag/AgCl reference electrode saturated with 3.0 M KCl. The potential measured by the Ag/AgCl reference electrode was converted into a reversible hydrogen electrode (RHE) potential using the formula:
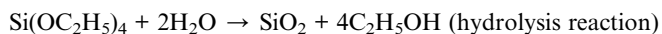
$$E_{\mathrm{RHE}} = E_{\mathrm{Ag/AgCl}} + 0.059\mathrm{pH} + E^0_{\mathrm{Ag/AgCl}}$$

where $E^0_{\mathrm{Ag/AgCl}}$ is 0.1976 V at 25 °C, and $E_{\mathrm{Ag/AgCl}}$ is the experimentally measured potential *vs.* the Ag/AgCl electrode. The photocurrent density measurement (*J–V* curve) was performed between −0.35 and 0.6 V *vs.* Ag/AgCl with a rate of 20 mV s^{-1}. The transient *J–V* curve was obtained by applying an external potential of 1.23 V *vs.* RHE, where the solar water splitting occurs. A shutter was used in every second term.

Results and discussion

Schematic drawings of the experimental procedures and the fabricated structures of the SiO$_2$ ultrathin under-layered Ti

15724 | *J. Mater. Chem. A*, 2015, **3**, 15723–15728

This journal is © The Royal Society of Chemistry 2015

doped hematite film and Ti doped hematite film on the FTO substrate are shown in Fig. S2(a).† Optical images of each sample are shown in Fig. S2(b).† Tetraethyl orthosilicate (TEOS), which was used as a Si precursor for the SiO_2 under-layer, was transformed into SiO_2 by the following hydrolysis reaction and thermal reaction:

$$Si(OC_2H_5)_4 + 2H_2O \rightarrow SiO_2 + 4C_2H_5OH \text{ (hydrolysis reaction)}$$

$$Si(OC_2H_5)_4 \rightarrow SiO_2 + 2(C_2H_5)_2O \text{ (thermal reaction)}[28]$$

Through these reactions, TEOS was deposited on the surface of the FTO substrate and a SiO_2 ultrathin layer was formed during the DA cycles. Considering the phase diagram of SiO_2 and the deposition conditions, the ultrathin SiO_2 layer exists on the FTO surface in an α-quartz state.[29]

In the TEM image in Fig. 1(a), the small sized SiO_2 particles were aggregated together and became an ultrathin SiO_2 layer on the FTO substrate. Based on the SiO_2 under-layer thickness of *ca.* 2–3 nm after one deposition, the thickness of the SiO_2 under-layer was increased to *ca.* 10 nm when the Si precursor was deposited three times on the FTO substrate (Fig. S3(a, a-1 and a-2)†). The SiO_2 layer with *ca.* 3 nm thickness was used as a new substrate to prepare a Ti doped hematite film. The cross-sectional TEM image of the SiO_2 under-layered Ti doped hematite is given in Fig. 1(b). The average thickness of the Ti doped hematite layer on the SiO_2 under-layered FTO substrate was *ca.* 50 nm. The hematite particles were aggregated and formed the Ti doped hematite film along the surface of the SiO_2 under-layered FTO substrate (Fig. S3(b, b-1 and b-2)†).

The binding state of the SiO_2 under-layer was revealed by XPS analysis. In the XPS Si 2p spectrum of the SiO_2 under-layer, the binding energy of Si was determined to be 102.2 eV, which matches well with the binding energy of typical SiO_2 (Fig. 2(a)).[30] The XPS survey scan of the SiO_2 under-layered Ti doped hematite film is given in Fig. S4(a).† The amount of Ti atoms in the SiO_2 under-layered Ti doped hematite film was *ca.* 7% (atomic ratio). The Ti 2p binding energies were 528.1 eV for Ti $2p_{3/2}$ and 464 eV for Ti $2p_{1/2}$. These values are similar binding energies as those in the Ti^{4+} state (Fig. S4(b)†). The Fe 2p XPS

spectrum showed binding energies at 724.2 eV for Fe $2p_{1/2}$ and 711 eV for Fe $2p_{3/2}$ with satellite peaks. These are the typical values observed for hematite (Fig. S4(C)†).[18] In the case of the Si 2p spectrum, the binding energy of Si was decreased compared with the binding energy of the SiO_2 under-layer (Fig. S4(d)†). The decreased binding energy was caused by the doped Si atoms in the bottom layer of the Ti doped hematite film. The specific structure of the SiO_2 under-layered Ti doped hematite film was revealed by XPS depth profiling (Fig. S4(e), (f)† and 2(b)). As the Ar etching number increased, the intensity of the Ti 2p spectra decreased without any shift in the peak position. This indicates that most of the Ti atoms exist on the surface of the hematite film (Fig. S4(e)†).[18] In the case of the Fe 2p spectra, the intensity of the peaks decreased as the Ar etching time increased (as the hematite film was etched out from the FTO surface) (Fig. S4(f)†). In the Si 2p spectra, as the etching time increased, the binding energy shifted from the doped Si state in the hematite (100 eV) to Si in the FTO substrate state (112 eV) *via* the SiO_2 under-layer state (102.5 eV) (Fig. 2(b)). According to these XPS depth profiling data, the structure of the SiO_2 under-layered Ti doped hematite film was assumed to be a layer by layer structure of the FTO substrate, the ultrathin SiO_2 under-layer and the Ti doped hematite film. The TEM EDXS point analysis also confirmed this structure. Comparing three points in the SiO_2 under-layered Ti doped hematite film (point 1 for the Ti doped hematite film, point 2 for the interface between hematite and the FTO substrate, and point 3 for the inside of the FTO substrate – see Fig. S5(a)†), the highest atomic percentage of Fe was recorded at point 1 and the value decreased when moving away from the surface of the hematite thin film. The atomic percentage of Ti was also highest at the surface of the Ti doped hematite film, which matches well with the previous XPS depth profiling data. The highest atomic percentage of Sn was recorded at point 3, inside the FTO substrate, and the value decreased as you moved closer to the surface of the Ti doped hematite thin film. In the case of Si, the highest Si atomic percentage was observed in between the FTO substrate and the Ti doped hematite thin film, at point 2, where the SiO_2 under-layer exists. However, similar to the XPS depth profiling data, some of the Si atoms also exist inside the Ti doped hematite thin film in the doped state and inside the FTO substrate as an impurity (Fig. S5(b) and (c)†).

By inserting an ultrathin SiO_2 under-layer between the FTO substrate and the hematite thin film, the photocurrent density increased from 0.17 mA cm^{-2} to 0.58 mA cm^{-2} at 1.23 V *vs.* RHE (Fig. 3(a)). In the case of the Ti doped hematite thin film, the photocurrent density jumped from 0.62 mA cm^{-2} to 0.76 mA cm^{-2} at 1.23 V *vs.* RHE after introducing the SiO_2 under-layer. Although the inserted SiO_2 under-layer led to an enhancement in the PEC activity of the hematite film, the thickness of the SiO_2 under-layer is an important factor because SiO_2 is an insulator. If the SiO_2 under-layer is too thick, the electron flow from the hematite thin film to the FTO substrate is also suppressed and no current will be measured because the thick SiO_2 under-layer blocks the electron flow. The thickness of the SiO_2 under-layer can be controlled by the concentration of the TEOS solution and the number of DA cycles (Fig. S6(a)†). The photocurrent density
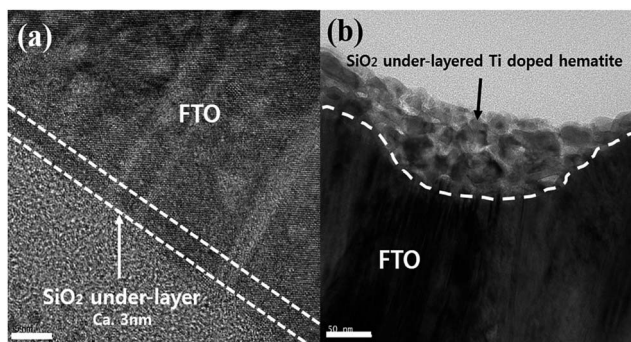

Fig. 1 Cross-sectional TEM images of (a) SiO_2 under-layer (with 5 nm scale bar), and (b) SiO_2 under-layered Ti doped hematite (with 50 nm scale bar).
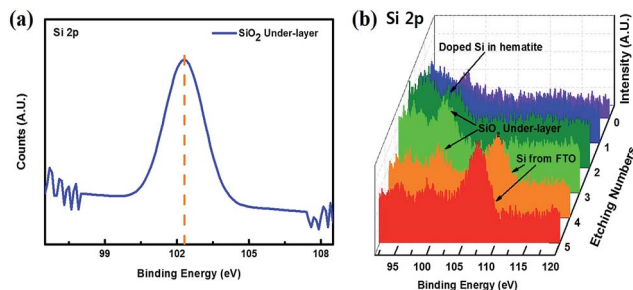
Fig. 2 (a) XPS Si 2p spectrum for the SiO_2 under-layer and (b) XPS Si 2p depth profile for the SiO_2 under-layered Ti doped hematite film.

Fig. 3 (a) Photocurrent density curves (J–V curves) of the pure hematite, Ti doped hematite, SiO_2 under-layered hematite and SiO_2 under-layered Ti doped hematite films. (b) APCE curves of pure hematite, Ti doped hematite and the SiO_2 under-layered Ti doped hematite film.

curves of the SiO_2 under-layered Ti doped hematite film with different concentrations of TEOS from 0.12 M to 1.35 M with one DA cycle between the FTO substrate and the Ti doped hematite film are shown in Fig. S6.† A TEOS concentration of 0.45 M as the Si precursor was the optimal concentration of TEOS to achieve the highest photocurrent value of 0.76 mA cm^{-2} at 1.23 V *vs.* RHE. If the thickness of the SiO_2 under-layer increased from *ca.* 3 nm to *ca.* 10 nm after 3 DA cycles with the TEOS precursor solution (Fig. S3(a, a-1 and a-2)),† the photo-current density of the Ti doped hematite film decreased (Fig. S6(b)†). The SiO_2 under-layered Ti doped hematite film showed the highest IPCE value of 6% with 380 nm mono-chromatic light, whereas the pure hematite film and Ti doped hematite film showed values of 0.2% and 5%, respectively (Fig. S7(a)†). However, the SiO_2 under-layered Ti doped hematite film showed the lowest absorbance compared to the Ti doped hematite film and pure hematite film (Fig. S7(b)†). Although the optical absorbance of the SiO_2 under-layered Ti doped hematite film is low due to scattering and reflection, the introduced SiO_2 under-layer can utilize the absorbed light more efficiently. The SiO_2 under-layered hematite film showed an APCE value of 14% with 380 nm monochromatic light, whereas the pure hematite thin film and Ti doped hematite thin film showed values of 0.3% and 10%, respectively (Fig. 3(b)). This is due to the suppression of back electron transfer from the FTO layer to the hematite layer, which suppresses the charge recombination. The band gaps assigned by the Tauc plots, calculated from UV-Vis spectroscopy, are given in Fig. S8.† The pure hematite film has a band gap energy of 2.0 eV, and the band gap energy was changed to 2.05 eV when Ti was doped into the pure hematite. When the SiO_2 under-layer was introduced into the Ti doped hematite, the bang gap energy increased to 2.1 eV. These bang gap energies match the typical bang gap energy of hematite (*ca.* 2.2 eV).[8] Minor band gap changes indi-cate that hematite maintains its original chemical characteris-tics, even when Ti was doped into the hematite thin film and the SiO_2 under-layer was introduced to the hematite thin film.

The enhanced PEC activity and APCE values are also caused from decreased impedance values. Fig. 4(a) shows Nyquist plots for the pure hematite film, Ti doped hematite film and SiO_2 under-layered Ti doped hematite film. The impedance value of the pure hematite film is 7000 Ohm. When Ti was doped into the pure hematite film, the impedance value decreased to
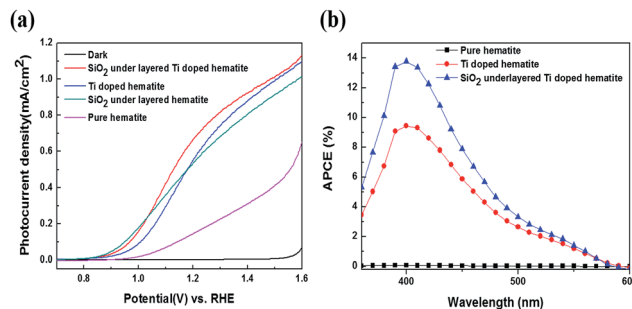
1600 Ohm. A further decreased impedance value of 1100 Ohm was obtained when the ultrathin SiO_2 under-layer was inserted between the FTO substrate and the Ti doped hematite film. When the ultrathin SiO_2 under-layer was inserted between the FTO substrate and the Ti doped hematite film, the impedance value decreased by 5900 Ohm compared to the pure hematite film. The decreased impedance value is a clue for the increased photocurrent density in the silica layered Ti doped hematite thin film. The decreased impedance value can be interpreted as the increased net driving force of the forward electron transfer *versus* the backward electron transfer due to the slightly increased energy barrier by the inserted SiO_2 layer. The effect of the SiO_2 under-layer also appeared in the transient J–V curve (Fig. 4(b)), where the reverse current appeared when the inci-dent light was turned off. A decrease in the reverse current from -0.075 mA cm^{-2} to -0.035 mA cm^{-2} was observed when the SiO_2 under-layer was introduced into the Ti doped hematite film. This is clearly shown in the reverse current magnified transient J–V curve given in Fig. S9.† The average surface roughness value of the SiO_2 under-layered Ti doped hematite film, measured with atomic force microscopy, was determined to be 1.62 nm and this is lower than the average surface roughness of the pure hematite film (34 nm) and Ti doped hematite film (31.1 nm). This indicates that the larger surface area of the hematite thin film does not critically influence the photocurrent value. It might be possible to conclude that the increased photocurrent value is critically influenced by the electron transporting ability of the hematite thin films, not due to the high surface area but due to the roughness of the hematite thin films (Fig. S10†).

Schematic drawings of the mechanisms for the decreased reverse current and enhanced PEC activity of the SiO_2 under-layered Ti doped hematite film are tentatively suggested in Scheme 1. In the case of the Ti doped hematite film, irradiation of light generates excited electrons in the conduction band of hematite (path ① in Scheme 1). These excited electrons flow to the FTO substrate and make the current flow (path ③ in Scheme 1), which can be determined by the current flow in the J–V curve. However, there are two possible pathways for electron–hole recombination in the Ti doped hematite film. The excited

15726 | *J. Mater. Chem. A*, 2015, **3**, 15723–15728
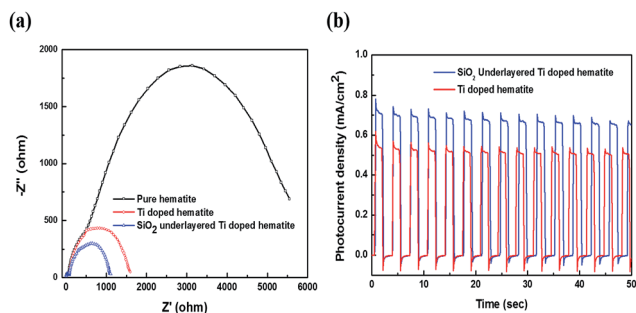
This journal is © The Royal Society of Chemistry 2015

Fig. 4 (a) EIS of the pure hematite, Ti doped hematite and SiO₂ under-layered Ti doped hematite films. (b) Transient *J–V* curves of SiO₂ under-layered Ti doped hematite and Ti doped hematite.

Scheme 1 Schematic drawings of the suggested mechanisms for the role of the ultrathin SiO₂ under-layer in the SiO₂ under-layered Ti doped hematite film.

electrons can recombine with holes inside the Ti doped hematite film (path ② in Scheme 1) or reversely flow from the FTO to the Ti doped hematite to recombine with holes in the Ti doped hematite (path ④ in Scheme 1).[23] The SiO₂ ultrathin insulating under-layer can suppress the recombination path ④, which is the reverse electron flow from the FTO to the Ti doped hematite layer. This is clearly shown by the reducing reverse current in the transient *J–V* curve in Fig. S9.† The Ti doped hematite photoanode can function as a diode system. These results are similar to those reported by Zhang *et al.*, who introduced a TiO₂ under-layer between a Pt-coated FTO and hematite film.[22] However, in this work, a greater suppression of the reverse electron recombination was achieved due to the insulator characteristics of the SiO₂ under-layer.

In addition, introducing the ultrathin SiO₂ under-layer between the Ti doped hematite film and the FTO substrate means that the Si atoms in the under-layer can diffuse into the Ti doped hematite film during the annealing procedure. The EXAFS spectrum of the pure hematite was refined with the IFEFFIT algorithm calculation (Fig. S11),† which matched well with the calculated fitting plot.[31] Introducing the ultrathin SiO₂ under-layer resulted in crystal distortion in the hematite thin film, which is represented by the increased distance between the Fe atom and Fe atom in the refined EXAFS spectrum in Fig. 5(a). When the Si atoms replaced the Fe positions by doping, the bond length between the Fe atom and Si atom decreases due to the lower electronegativity of the Si atom.[32] The

decreased bond length between the Fe atom and Si atom increased the bond length between the Fe atom and Fe atom with distortion of the crystal structure in the Ti doped hematite film (Fig. 5(b)). The electron localization around the Fe atoms was increased by the diffused Si atoms *via* the SiO₂ under-layer distortion of the crystal structure of hematite, inducing an increase in the electron density around the central Fe atoms in the XANES, which was refined from the XAFS spectra in Fig. S12(a).† The XANES white lines of pure hematite, Ti doped hematite, SiO₂ under-layered hematite and SiO₂ under-layered Ti doped hematite are given in Fig. S12(b).† After the SiO₂ under-layer was introduced between the FTO substrate and the hematite film, the white line energy of the central Fe atom moved *ca.* ∼2 eV in the lower energy direction, which equates to a reduction of the central Fe atoms. The rich electron density around the Fe atoms enhanced the electron mobility through the Fe atoms, contributing to an enhancement in the PEC activity of both the hematite film and Ti doped hematite film.

Conclusions

An ultrathin SiO₂ under-layer with a thickness of *ca.* ∼3 nm was introduced between the FTO substrate and the hematite thin film. By introducing the ultrathin SiO₂ under-layer, the reverse current during the PEC water splitting reaction was reduced and it resulted in the suppression of the electron–hole recombination pathway from the FTO substrate to the hematite thin film. An enormous increase in the PEC activity was obtained for the Ti doped hematite film with a promising photocurrent density of 0.76 mA cm^{-2} at 1.23 V *vs.* RHE under 1 sun illumination without any hole scavenger materials and co-catalysts. Thus, this work reports a new way to apply insulator materials as an under-layer to achieve an enhanced PEC activity of the base materials during the solar water splitting reaction.
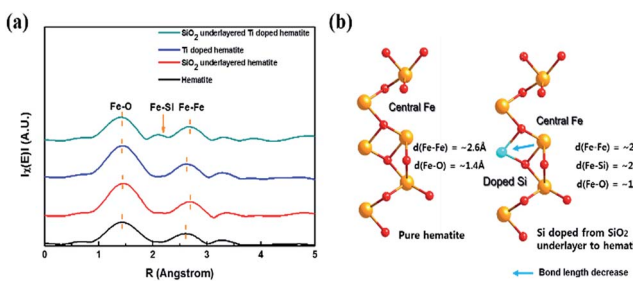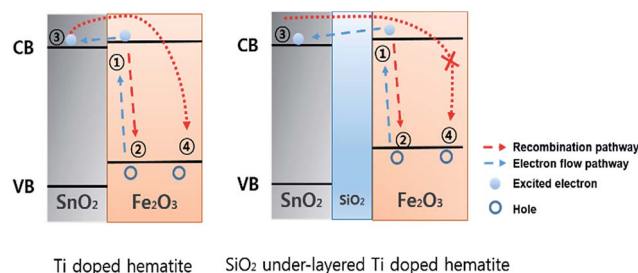
Acknowledgements

Fig. 5 (a) Refined EXAFS analysis of the pure hematite, Ti doped hematite, SiO₂ under-layered hematite and SiO₂ under-layered Ti doped hematite films. (b) Schemes for the atomic structure of Si doping in the SiO₂ under-layer in the SiO₂ under-layered hematite.

This journal is © The Royal Society of Chemistry 2015

J. Mater. Chem. A, 2015, 3, 15723–15728 | 15727

Notes and references

1 S. Bensaid, G. Centi, E. Garrone, S. Perathoner and G. Saracco, *ChemSusChem*, 2012, **5**, 500.

2 M. S. Prevot and K. Sivula, *J. Phys. Chem. C*, 2013, **117**, 17879.

3 M. G. Walter, E. L. Warren, J. R. Mckone, S. W. Boettcher, Q. Mi, E. A. Santori and N. S. Lewis, *Chem. Rev.*, 2010, **110**, 6446.

4 S. Hu, C. Xiang, S. Haussener, A. D. Berger and N. S. Lewis, *Energy Environ. Sci.*, 2013, **6**, 2984.

5 M. Grätzel, *Nature*, 2001, **414**, 338.

6 T. W. Kim and K. S. Choi, *Science*, 2014, **343**, 990.

7 A. Wolcott, W. A. Smith, T. R. Kuykendall, Y. Zhao and J. Z. Zhang, *Adv. Funct. Mater.*, 2009, **19**, 1849.

8 A. Duret and M. Grätzel, *J. Phys. Chem. B*, 2005, **109**, 17184.

9 K. Sivula, F. L. Formal and M. Grätzel, *ChemSusChem*, 2011, **4**, 432.

10 O. Khaselev and J. A. Turner, *Science*, 1998, **280**, 425.

11 N. J. Cherepy, D. B. Linston, J. A. Lovejoy, H. Deng and J. Z. Zhang, *J. Phys. Chem. B*, 1998, **102**, 770.

12 Y. Lin, Y. Xu, M. T. Mayer, Z. I. Simpson, G. McMahon, S. Zhou and D. Wang, *J. Am. Chem. Soc.*, 2012, **134**, 5508.

13 D. K. Zhong, M. Cornuz, K. Sivula, M. Grätzel and D. R. Gamelin, *Energy Environ. Sci.*, 2011, **4**, 1759.

14 M. Marelli, A. Naldoni, A. Muinguzzi, M. Allieta, T. Virgili, G. Scavia, S. Recchia, R. Psaro and V. D. Santo, *ACS Appl. Mater. Interfaces*, 2014, **6**, 11997.

15 G. M. Carroll, D. K. Zhong and D. R. Gamelin, *Energy Environ. Sci.*, 2015, **8**, 577.

16 J. Y. Zheng, S. I. Son, T. K. Van and Y. S. Kang, *RSC Adv.*, 2015, **5**, 36307.

17 M. E. A. Warwick, D. Barreca, E. Bontempi, G. Carraro, A. Gasparotto, C. Maccato, K. Kaunisto, T.-P. Ruoko, H. Lemmetyinen, C. Sada, Y. Gonullu and S. Mathur, *Phys. Chem. Chem. Phys.*, 2015, **17**, 12899.

18 Y. Ling, G. Wang, D. A. Wheeler, J. Z. Zhang and Y. Li, *Nano Lett.*, 2011, **11**, 2119.

19 H. G. Cha, M. J. Kang, I. C. Hwang, H. Kim, K. B. Yoon and Y. S. Kang, *Chem. Commun.*, 2015, **51**, 6407.

20 Y. Lin, S. Zhou, S. W. Sheehan and D. Wang, *J. Am. Chem. Soc.*, 2011, **133**, 2398.

21 D. Barreca, G. Carraro, A. Gasparotto, C. Maccato, C. Sada, A. P. Singh, S. Mathur, A. Mettenborger, E. Bontempi and L. E. Depero, *Int. J. Hydrogen Energy*, 2013, **38**, 14189.

22 I. Cesar, A. Kay, J. A. G. Martinez and M. Grätzel, *J. Am. Chem. Soc.*, 2006, **128**, 4582.

23 G. Wang, Y. Ling, D. A. Wheeler, K. E. N. George, K. Horsley, C. Heske, J. Z. Zhang and Y. Li, *Nano Lett.*, 2011, **11**, 3503.

24 K. Saroj, T. Chanakya, S. P. Aadesh, C. Diwakar, S. Rohit, D. Sahab and S. R. Vibba, *Curr. Sci.*, 2006, **91**, 1062.

25 H. Y. Sheng, K. S. Alan, A. J. Forman, D. Hazen, J. N. Park and E. W. McFarland, *Chem. Mater.*, 2008, **20**, 3803.

26 T. Hisatomi, H. Dotan, M. Stefik, K. Sivula, A. Rothschild, M. Grätzel and N. Mathews, *Adv. Mater.*, 2012, **24**, 2699.

27 D. Wang, X. Zhang, P. Sun, S. Lu, L. Wang, Y. Wei and Y. Liu, *Int. J. Hydrogen Energy*, 2014, **39**, 16212.

28 K. Kato, *J. Mater. Sci.*, 1992, **27**, 1445.

29 V. Swamy and S. K. Saxena, *J. Geophys. Res.*, 1994, **99**, 11787.

30 B. V. Crist, The Elements and Native Oxides, *Handbook of Monochromatic XPS spectra*, John Wiley & Sons Ltd, England, 2000, p. 466.

31 M. Newville, *J. Synchrotron Radiat.*, 2001, **8**, 322.

32 J. Hinze and H. H. Jaffe, *J. Am. Chem. Soc.*, 1962, **84**, 540.